Particuology 115 (2026) 47–54

Contents lists available at ScienceDirect

Particuology

journal homepage: www.elsevier.com/locate/partic

Lithium content effects on the phase evolution, microstructure and morphology of hydrothermally synthesized $Li_4Ti_5O_{12}$-TiO_2 nanocomposites

Hamed Aghamohammadi[a,*], Atousa Khazaeli[b], Reza Eslami-Farsani[b]

[a] Department of Advanced Materials and New Technologies, Iranian Research Organization for Science and Technology (IROST), Tehran, Iran
[b] Faculty of Materials Science and Engineering, K. N. Toosi University of Technology, Tehran, Iran

HIGHLIGHTS

- Effects of different $LiOH{\cdot}H_2O$:TBT ratios on the hydrothermal synthesis of LTO-TiO_2 investigated.
- Phase, microstructure, and morphology of the samples were studied.
- Phase evolution occurred by increasing the Li precursors ratios.
- LTO crystallite size reduced from 40nm to 20–21 nm with increasing Li content.
- Higher Li ratios favor LTO-TiO_2 rutile nanocomposites with refined morphology.

GRAPHICAL ABSTRACT

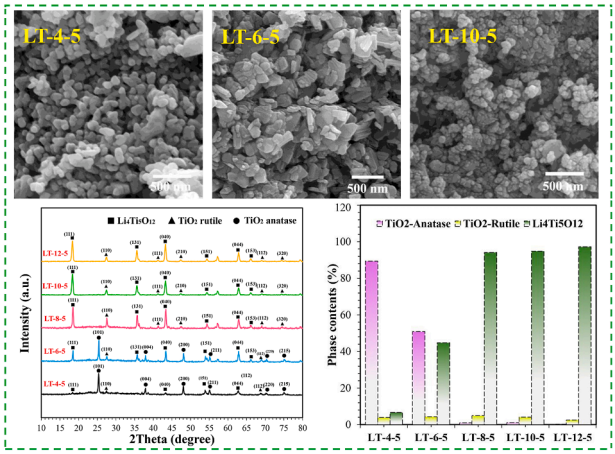

ARTICLE INFO

Keywords:
$Li_4Ti_5O_{12}$-TiO_2 nanocomposite
Hydrothermal synthesis
Lithium precursor ratio
Microstructure
Morphology

ABSTRACT

$Li_4Ti_5O_{12}$-TiO_2 nanocomposites represent highly promising materials for energy storage applications owing to their attractive electrochemical properties. However, precisely optimizing their morphology and compositions is essential. In this study, the effects of lithium content on the synthesis of the $Li_4Ti_5O_{12}$-TiO_2 nanocomposites prepared by the hydrothermal method were investigated. The samples were prepared using different molar ratios of $LiOH{\cdot}H_2O$: tertbutyl titanate (TBT) (4:5, 6:5, 8:5, 10:5, and 12:5) using a hydrothermal process at 180 °C for 12 h, followed by a calcination step. The microstructure, phase analysis, and morphology of the samples were investigated using X-ray diffraction (XRD), Raman spectroscopy, and field-emission scanning electron microscopy (FESEM) analyses. XRD results showed a phase evolution from an anatase-rich TiO_2 (at a ratio of 4:5) to a $Li_4Ti_5O_{12}$-dominated nanocomposite (at a ratio of 12:5) with a minor TiO_2 rutile phase. Also, the crystallite size of the $Li_4Ti_5O_{12}$ phase first increased to a maximum value of 47.3 nm and then decreased to 20–21 nm at higher ratios. FESEM images revealed a growth in particle size of the samples from 138 to 196 nm, by increasing the ratio from 4:5 to 6:5, and then a reduction of particle size to about 55 nm by using higher ratios. The results

* Corresponding author.
E-mail addresses: aghamohammadi@irost.ir, hamed.aghamohammadi@outlook.com (H. Aghamohammadi).

https://doi.org/10.1016/j.partic.2026.05.003
Received 12 April 2026; Received in revised form 6 May 2026; Accepted 8 May 2026
Available online 12 May 2026

showed that for achieving $Li_4Ti_5O_{12}$-TiO_2 rutile nanocomposites with nanoscale particles, higher LiOH·H_2O:TBT ratios are preferred.

1. Introduction

Spinel LTO, as a common type of titanium-based materials, with a general formula of $Li_4Ti_5O_{12}$ owing to its structural stability, negligible volume change during charge/discharge, and safe operating potential (~1.55 V vs. Li/Li^+) has been widely studied as an anode material for lithium-ion batteries (LIBs). However, their low conductivity restricts their rate capability performance in LIBs (Aghamohammadi & Eslami-Farsani, 2022; Aghamohammadi et al., 2024; Aghamohammadi et al., 2021; Chen et al., 2025a, 2025b, Kazemi et al., 2025; Parikh et al., 2021; Zhang et al., 2022).

Recent works have shown that the formation of LTO-TiO_2 nanocomposites can improve the electrochemical performance of LTO by various mechanisms (Gangaja et al., 2024a, 2024b, He, Chu, & Zhuo, 2021; Hwang et al., 2019; Xu et al., 2017; Zhang et al., 2016). For example, in the work of Gangaja et al. (2024a), a high capacity value of 203 mAh/g has been reported for LTO-TiO_2 nanocomposite at 1C, which was about 16% higher than the theoretical capacity value of LTO (175 mAh/g). In another study, Xu et al. (2017) synthesized LTO-TiO_2 nanocomposites with sheet-like morphology using hydrothermal treatment as anode materials for LIBs. The samples presented sheet-like morphology with length, width, and thickness of 1000, 500, and 3–50 nm, respectively. Their results showed that the presence of TiO_2 cannot increase the capacity beyond the intrinsic capacity of TiO_2, while the role of TiO_2 was growth-controller of the LTO particles and providing more grain boundaries, which serve as active sites for the diffusion of Li-ions. They reported that the capacity value of LTO increased from 162 to 182 mAh/g at a charge/discharge rate of 1C. However, to achieve the positive role of the TiO_2, its content should be optimized and controlled, so that the excess TiO_2 does not decrease the total capacity of the composite.

In another work conducted by Hwang et al. (2019), the LTO-TiO_2 rutile nanocomposites with polygonal morphology were prepared using the hydrothermal method. The rate capability results showed that LTO-TiO_2 rutile nanocomposites presented higher capacity values at all current densities compared to pure LTO and LTO-Li_2TiO_3 anodes. For example, at a charge/discharge rate of 5C, the LTO-TiO_2 rutile nanocomposites presented a capacity value of about 110 mAh/g, which was about 20% higher than that of pure LTO (about 90 mAh/g). The better electrochemical performance of the LTO-TiO_2 rutile nanocomposites can be attributed to the low diffusion barrier of the TiO_2 rutile along c-axis, shortening the solid-state diffusion length (Sushko et al., 2010).

Up to now, various methods such as sol-gel (Kuo & Lin, 2014; Michalska et al., 2022; Shen et al., 2003), solid-state (Wu et al., 2025; Zou et al., 2025), molten-salt (Hu et al., 2024; Muzayanha et al., 2021; Xie et al., 2021), hydro-solvothermal (Merazga et al., 2024; Winowatan et al., 2021; Zhang & Zhang, 2019; Zima et al., 2023) methods have been used for the synthesis of LTO materials. Hydro-solvothermal routes outperform conventional synthesis methods for LTO-based materials by delivering precise morphology control, and a high-purity process that is both simpler and cleaner. However, similar to all synthesis methods, the hydro-solvothermal methods should also be optimized to achieve the desired morphology and composition of the LTO-based nanocomposites.

The main parameters affecting hydro-solvothermal methods include the precursor composition, holding temperature, holding time, and calcination parameters. In the case of hydro-solvothermal synthesis methods, there are some papers in the literature regarding the effects of the synthesis parameters on the microstructure and morphology of the LTO. Although hydrothermal synthesis of LTO-TiO_2 composites and the influence of the Li:Ti ratio on phase formation have been investigated, the existing literature has largely focused on near-stoichiometric ratios. For example, Wu et al. (2017) synthesized dual-phase LTO-TiO_2 rutile nanosheets via hydrothermal treatment using Li:Ti ratios of 4.0:5 to 4.5:5, followed by calcination at 600 °C. In another work conducted by Xu et al. (2017), they reported a hydrothermal synthesis method for the preparation of LTO-TiO_2 nanocomposites. In their work, TBT and LiOH (at Li/Ti = 4.2:5) in glycerol were used as starting materials, and a hydrothermal process was conducted at 180 °C for 24 h, followed by calcination at different temperatures of 400-600 °C for 6h in air. Their results showed the formation of the LTO-TiO_2 anatase with sheet-like morphology at higher calcination temperatures while lower calcination temperature led to formation of pure LTO. However, a systematic investigation extending into the highly Li-excess regime remains absent in the literature. Furthermore, the quantitative mapping of phase contents and the non-monotonic evolution of crystallite size and morphology across broad Li:Ti ratios have not been reported. Therefore, this work aims to provide a comprehensive, and quantitative study of the effects of Li precursor content on phase evolution, crystallite size, and morphology of LTO-TiO_2 nanocomposites synthesized via a hydrothermal method followed by calcination at 700 °C. It is important to note that while LTO-TiO_2 composites are promising anode materials for LIBs, the present work does not claim to optimize electrochemical performance. Instead, the quantitative relationships between precursor composition, phase evolution, crystallite size, and particle morphology are investigated in this study.

2. Experimental procedure

In this study, to synthesize LTO-TiO_2 nanocomposites, LiOH·H_2O (Sigma Aldrich) and tetrabutyl titanate (TBT, Sigma Aldrich) were used as Li and Ti precursors, respectively. In this work, different molar ratios of the LiOH·H_2O: TBT (4:5, 6:5, 8:5, 10:5, and 12:5) were added to 70 ml of deionized (DI) water. After mixing for 30 min at 25 °C, the mixture was transferred to a 100 ml Teflon-lined stainless-steel autoclave. After that, the hydrothermal treatment was done at 180 °C for 12 h, and then, the collected powders were filtered and washed with DI water several times. The prepared powders were calcined under an air atmosphere at 700 °C for 5 h. The selection of hydrothermal and post-treatment temperatures in this study was based on previous optimization studies of the synthesis of LTO-based materials (Li et al., 2012; Liu et al., 2018; Zhu et al., 2016). The schematic illustration of the synthesis steps is presented in Fig. 1. Based on the ratios of precursors, the samples were named as LT-4-5, LT-6-5, LT-8-5, LT-10-5, and LT-12-5.

The structural and morphological analyses of the samples were studied using X-ray diffraction (XRD), Raman and field-emission scanning electron microscopy (FESEM). FESEM imaging was conducted using a MIRA3-TESCAN Czechia instrument. The XRD analysis (Rigaku Ultima IV, Japan) was performed by Cu Kα radiation and a step scan of 0.05° for the 2θ range of 10 – 80° It is worth noting that the phase analysis was performed with Highscore Plus software, while the quantitative analysis was performed with both MAUD software and Highscore Plus software. Moreover, Raman spectroscopy (TakRam N1-541, Teksan Co, Iran) with a laser wavelength of 532 nm was used to confirm the phase analysis of the samples.

3. Results and discussion

3.1. XRD analysis

In this work, the XRD analysis was used to investigate the phase analysis of the samples. Fig. 2 shows the XRD patterns of the samples prepared by the hydrothermal method. As can be observed, the LT-4-5

and LT-6-5 samples are mostly comprised of TiO_2 anatase with small contents of the $Li_4Ti_5O_{12}$ phase. However, by increasing the $LiOH{\cdot}H_2O$ content of the samples, the peaks related to TiO_2 anatase phase disappeared while the intensity of the peaks related to the TiO_2 rutile and $Li_4Ti_5O_{12}$ phases increased. The increase in the intensity of peaks related to $Li_4Ti_5O_{12}$ shows the increment of its contents in these samples.

The magnified XRD patterns of the samples are presented in Fig. 2 (b–d). As can be seen, by increasing the $LiOH{\cdot}H_2O$ content in the samples, the peaks generally shifted to the lower angles. Based on the Bragg equation ($n\lambda = 2d\sin\theta$), shifting to lower angles reveals the increment of the interplanar spacing and lattice expansion of the LTO. Because of the larger size of the Li-ion (with ionic radius of 0.76 Å) than the Ti^{4+} ion (with ionic radius of 0.605 Å), it can be deduced that the substitution of the Ti^{4+} with Li^{+} increased the d-spacing of LTO (Ariyoshi et al., 2005; Ge et al., 2008). Consequently, the higher contents of $LiOH{\cdot}H_2O$ promoted the formation of defective LTO-TiO_2 composites. As presented earlier, defective LTO provides more pathways for Li-ion transport, making it a more suitable anode material in LIBs. For example, in the work of Ge et al. (2008), the effects of Li-doping on the electrochemical performance of the LTO anodes for LIBs were investigated. Their results showed that the Li-doping caused an increase in specific capacity value of the LTO anode at all current densities owing to the increased electrical conductivity from 7.1×10^{-8} to 3.5×10^{-5} S/cm and increment of Li-ion diffusion coefficient from 2.1×10^{-9} to 2.5×10^{-9} cm^2/s. Accordingly, it can be deduced that the LT-10-5 and LT-12-5 samples are suitable for use as anode materials for LIBs, due to the higher degree of Li-doping in their structure.

The quantitative analysis of the LTO-TiO_2 samples is presented in Fig. 3. As can be seen in Fig. 3(a), the crystallite size of the LTO phase of the samples first increased by increasing the ratio of the $LiOH{\cdot}H_2O$: TBT from 4:5 to 6:5 and then decreased. In other words, the calculated crystallite sizes of the LT-4-5, LT-6-5, LT-8-5, LT-10-5, and LT-12-5 are respectively 40.2, 47.3, 28.7, 20.2, and 21.4 nm. The phase contents of the samples are presented in Fig. 3(b). It can be seen that LTO contents increased from 6.7% to 97.23% by increasing the $LiOH{\cdot}H_2O$: TBT from 4:5 to 12:5, while the TiO_2 anatase contents decreased from 89.36% to 0.2%. The TiO_2 rutile is present in low amounts in the range of 2.55% to 4.9%.

The non-linear evolution of the LTO crystallite size provides insight into the underlying nucleation and growth kinetics. In other words, at low Li:Ti ratios (in LT-4-5 and LT-6-5 samples), the low availability of Li-ions favors the preferential growth of TiO_2 anatase, while the emerging LTO phase coarsens via Ostwald ripening under moderate supersaturation. As the Li:Ti ratio increases beyond 6:5, the excess Li-ions adsorb onto the hydrated TiO_2 surface, generating anion vacancies that significantly increase the density of nucleation sites (Grzmil et al., 2004; Kim et al., 2022). The resultant high nucleation rate overcomes grain growth, leading to the refined crystallite sizes observed for LT-8-5, LT-10-5, and LT-12-5 samples. This competition between a growth-promoting effect and a nucleation-enhancing effect can be introduced as the possible reason for the observed highest value of crystallite size in LT-6-5 sample.

3.2. Raman analysis

The Raman spectrum of the LTO-TiO_2 samples is presented in Fig. 4. Fig. 4(a) presents the Raman spectrum of LT-4-5 that includes four fingerprint bands for TiO_2 anatase at 157 cm^{-1} (related to Eg mode arising from in-plane O–Ti–O bending), the 402 cm^{-1} (related to B_1g band produced by out-of-phase Ti–O bending perpendicular to the c-axis), the 514 cm^{-1} (A_1g/B_1g) feature dominated by Ti–O stretching along the c-axis, and the 638 cm^{-1} (Eg) overtone that reflects in-plane Ti–O stretching/bending motion of the TiO_6 octahedra. As can be seen in Fig. 4(b), similar peaks to those of LT-4-5 sample can be observed for the LT-6-5 sample, demonstrating the presence of the anatase phase as the dominant phase in this sample (Challagulla et al., 2017).

The Raman spectrum of LT-8-5 is presented in Fig. 4(c), which reveals the peaks related to $Li_4Ti_5O_{12}$ and TiO_2 rutile. The peaks related to LTO located at 237 cm^{-1} (F_2g, Li/Ti–O bending), 347 cm^{-1} (Eg, O–Ti–O bending in TiO_6), 443 cm^{-1} (F_2g, asymmetric Ti–O stretch) and 673 cm^{-1} (A_1g, TiO_6 breathing); the rutile fingerprints at 620 cm^{-1} (A_1g, O–Ti–O breathing) and anatase contributions recognized by the strongest Eg mode down-shifted to 157 cm^{-1} together with its companion at 520 cm^{-1} (B_1g/A_1g), confirming that the powder is a lithium-rich spinel core co-crystallized with both TiO_2 polymorphs. Fig. 4(d) presents the Raman spectrum of the LT-10-5 specimen, in which five distinct bands are resolved at 237, 353, 443, 614, and 673 cm^{-1}. The first four features are the characteristic phonon signatures of spinel LTO, with the 237 cm^{-1} F_2g mode arising from coupled Li–O and Ti–O bending motions, the 353 cm^{-1} Eg band corresponding to symmetric O–Ti–O bending within the TiO_6 octahedra, the 443 cm^{-1} F_2g feature stemming from asymmetric Ti–O stretching, and the intense 673 cm^{-1} A_1g peak originating from the breathing vibration of the TiO_6 units. The remaining band at 614 cm^{-1} is attributed to the A_1g breathing mode of TiO_2 rutile, corroborating the two-phase composition inferred from XRD analysis. Similar peaks can also be observed for the LT-12-5 sample (Challagulla et al., 2017; Tran et al., 2016; Xue et al., 2019). From these observations, it can be deduced that by increasing the $LiOH{\cdot}H_2O$: TBT ratio, first the anatase phase changes to rutile, and then by increasing the ratio, the LTO-TiO_2 (rutile) phase is formed through hydrothermal treatment followed by calcination at 700 °C in an air atmosphere.

3.3. Morphology of samples

In this section, the morphologies of the samples are evaluated. Fig. 5 shows the FESEM images of the LT-4-5 samples at different magnifications along with size distribution analysis. As can be observed, this

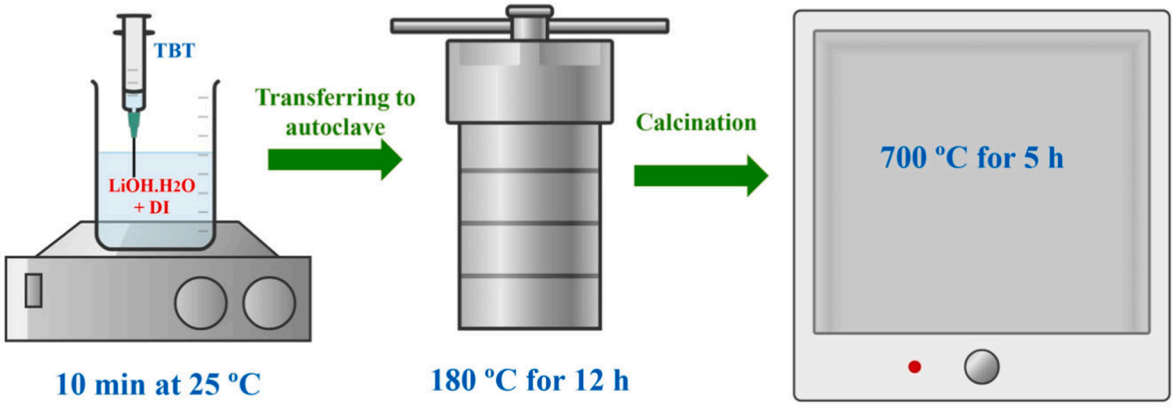

Fig. 1. Schematic image of hydrothermal synthesis steps for preparation of LT-TiO_2 samples.

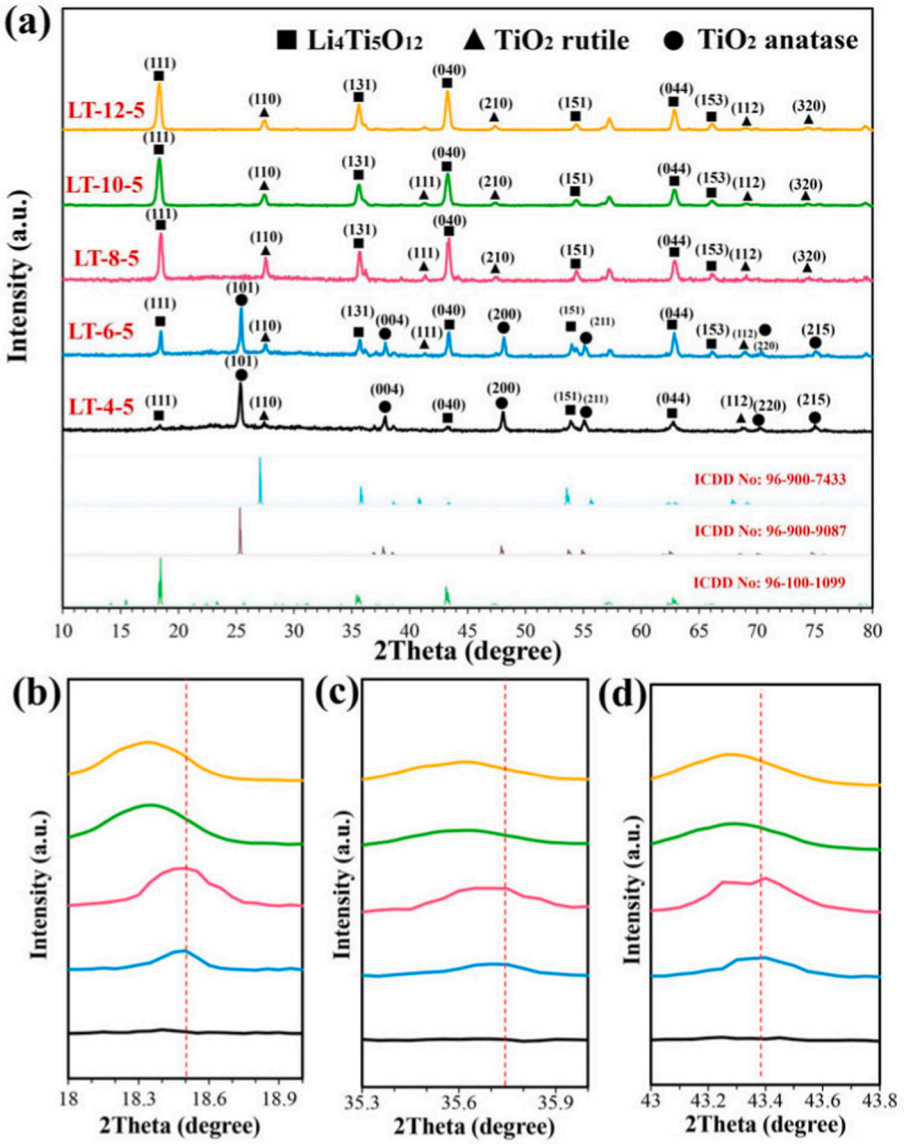

Fig. 2. XRD analysis of the hydrothermally synthesized samples, (a) general XRD patterns, (b to d) magnified XRD patterns.

sample consisted of particles with an average particle size of 138 nm. As shown, the majority of the particles are in the size ranges of 65-134 nm (58%) and 134-203 nm (29%).

The FESEM images of the LT-6-5 samples at different magnifications, along with size distribution analysis, are presented in Fig. 6. In this sample, the sheet-like morphology and near-spherical shape can be observed. According to Fig. 6(c), it can be seen that the average particle size increased to 196 nm, and the majority of the particles are in the size range of 147-216 nm (49%). These results are in agreement with XRD results, and as indicated, the crystallite size of the phase in the LT-6-5

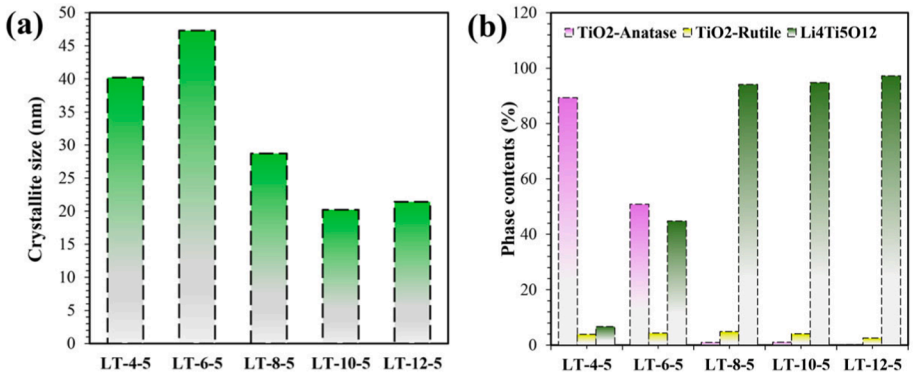

Fig. 3. Quantitative analyses of the samples, (a) crystallite size of the LTO phase, and (b) phase contents of the samples.

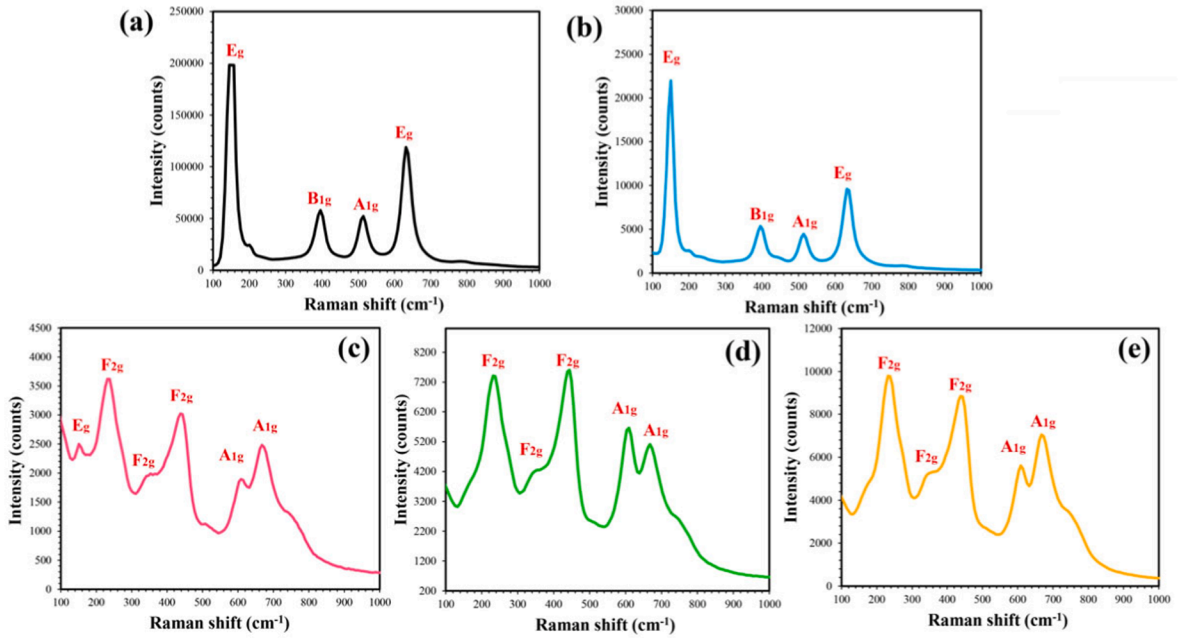

Fig. 4. The Raman spectrum of the (a) LT-4-5, (b) LT-6-5, (c) LT-8-5, (d) LT-10-5 and (e) LT-12-5 samples.

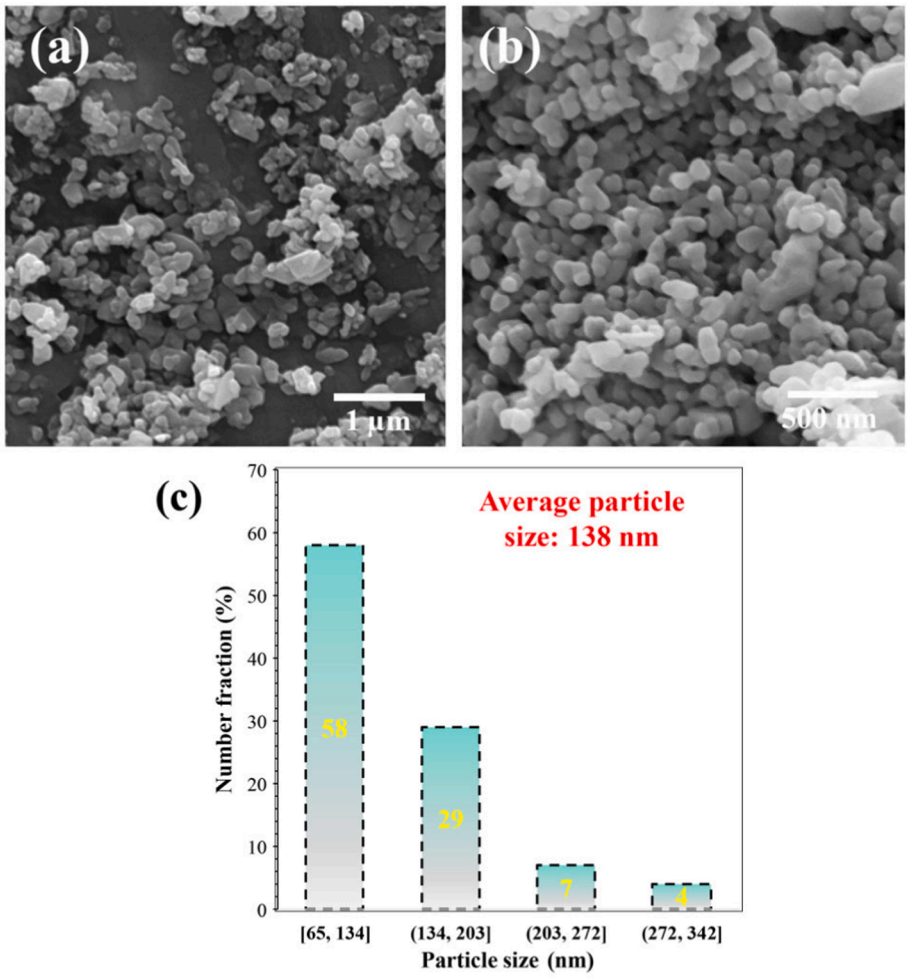

Fig. 5. (a, b) FESEM images and (c) size distribution of LT-4-5 sample.

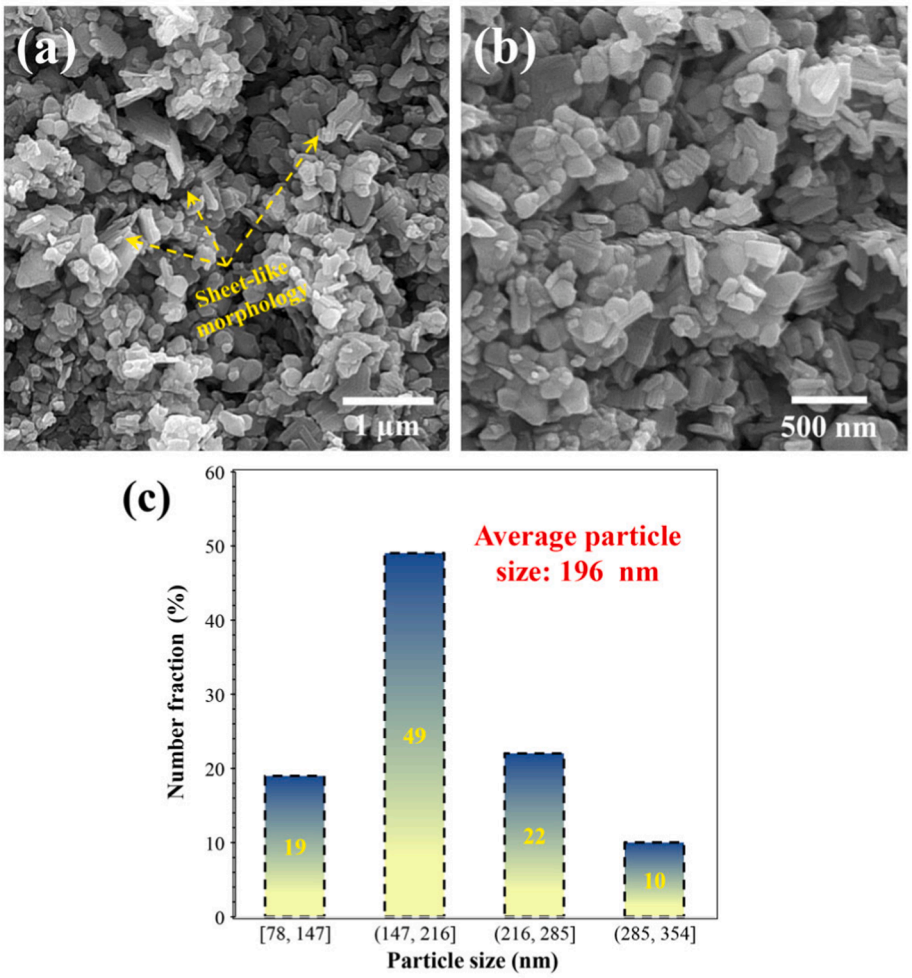

Fig. 6. (a, b) FESEM images and (c) size distribution of the LT-6-5 sample.

sample was the highest among the samples. It is important to note that the smaller size calculated using the XRD method compared to FESEM images is related to the fact that the XRD method calculates the individual crystallite while the FESEM images show secondary particles that are typically aggregates into multiple crystallites. The aggregation of primary crystallites into larger secondary particles is common in hydrothermally synthesized oxide materials, where surface energy minimization drives the assembly of nanocrystalline domains during the solvothermal and calcination steps (Li, Han, et al., 2012).

The FESEM images of the LT-10-5 samples at different magnifications, along with the size distribution analysis, are depicted in Fig. 7. As can be observed, there is no sign of sheet-like morphology in this sample and the average particle size of 55 nm was obtained. From these observations, it can be deduced that the increment of $LiOH{\cdot}H_2O$ content in the sample firstly resulted in increasing the particle size, while with higher contents, it led to the formation of small-sized particles. From XRD results, it can be concluded that when the ratio of the $LiOH{\cdot}H_2O$: TBT is low (i.e., 4:5 and 6:5), particle growth occurred in the TiO_2 anatase. While by increasing the $LiOH{\cdot}H_2O$: TBT (i.e. 10:5 and 12:5) and phase evolution to LTO and TiO_2 rutile, the particle growth was inhibited. In other words, Li-ions accelerated the nucleation and prevented the formation of sheet-like morphology.

4. Proposed mechanism for phase evolution

As shown by structural results, a phase evolution phenomenon occurred by increasing the $LiOH{\cdot}H_2O$: TBT ratios from low (LT-4-5 and LT-6-5) to higher ratios (LT-10-5 and LT-12-5). Accordingly, in this section, possible phase evolution mechanisms based on our observations are proposed. As mentioned in the experimental section, the TBT and $LiOH{\cdot}H_2O$ were mixed first in DI water. The first step is the hydrolysis of the TBT to form TiO_2. In this step, the TBT is first hydrolyzed to $Ti(OH)_4$ species and then transformed to TiO_2 by a condensation step as presented in the following hydrolysis (eq. (1)) and condensation reaction (eq. (2)):

$$Ti(OC_4H_9)_4 + 4H_2O \rightarrow Ti(OH)_4 + 4C_4H_9OH \quad (1)$$

$$Ti(OH)_4 \rightarrow TiO_2\ (anatase) + 2H_2O \quad (2)$$

Among the various polymorphs of TiO_2, the probability for the formation of anatase is higher than that of other polymorphs, such as rutile, owing to its more open framework. After that, through a hydrothermal process, the $LiOH{\cdot}H_2O$ reacts with TiO_2 anatase to form an amorphous $Li_4Ti_5O_{12}{\cdot}xH_2O$ hydrous layer on TiO_2 and then, through calcination steps, the reaction is completed as follows:

$$4LiOH + 5TiO_2\ (anatase) \rightarrow Li_4Ti_5O_{12} + 2H_2O \quad (3)$$

During the calcination step, two competing processes of the completion of spinel LTO formation via solid-state ion diffusion, and the anatase to rutile polymorphic transformation occur. From another viewpoint, the occurred phase evolution can be also explained through ion-exchange kinetics and thermodynamic stability. During the hydrothermal stage, intercalation of Li-ion into the framework of TiO_2 anatase leads to the formation of metastable layered intermediates (Li, Han,

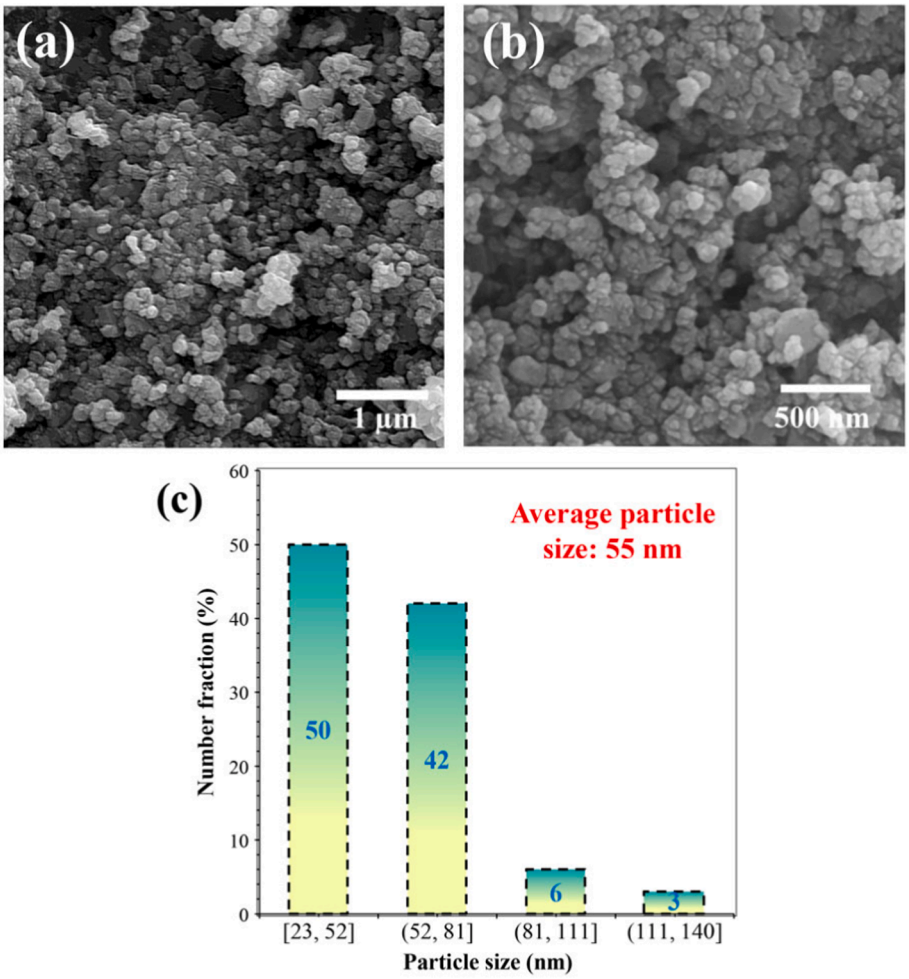

Fig. 7. (a, b) FESEM images and (c) size distribution of LT-10-5 sample.

et al., 2012). After the calcination process, these intermediates undergo dehydration and structural rearrangement to form spinel LTO. Simultaneously, the transformation of anatase to rutile occurs via a reconstructive mechanism involving about 8% volume shrinkage and Ti–O bond breaking (Hanaor et al., 2012). Previous studies have shown that TiO_2 rutile is thermodynamically stable at all temperatures, while anatase is metastable but kinetically stabilized by its lower surface energy (Hanaor et al., 2012; Kim et al., 2022). The persistence of rutile TiO_2 even at high Li:Ti ratio (LT-12-5) proves that this transformation is thermodynamically favored. According to the study of Grzmil et al. (2004), Li-ion adsorption on hydrated TiO_2 stabilizes anion vacancies, lowering the activation barrier for rutile nucleation. The higher calcination temperature employed in this work provides sufficient thermal energy to drive this transformation before complete lithiation to spinel LTO can occur.

Moreover, according to the phase content analysis, the applied approach in this work led to the formation of ternary composites with phase boundaries/heterojunctions. Based on the XRD peak shifting to lower angles, it can be concluded that the Li-ion substitution and consequent formation of defective interfaces occurred for the LTO-TiO_2 nanocomposites prepared in this work. According to the work of Xu et al. (2017), the grain/phase boundaries in these ternary nanocomposites act as channels for Li-ion diffusion and reservoirs for oxygen vacancies, improving electrical conductivity, which is beneficial for energy storage applications (Ariyoshi et al., 2005; Ge et al., 2008; Rahman et al., 2011).

5. Conclusion

In this study, the effects of different $LiOH{\cdot}H_2O$: tetrabutyl titanate (TBT) molar ratios (4:5, 6:5, 8:5, 10:5, and 12:5) on the phase, microstructure and size and morphology of the $Li_4Ti_5O_{12}$ (LTO)-based nanocomposites prepared by hydrothermal method were investigated. The main conclusions of this work are as follows:

(1) The XRD results showed that increasing $LiOH{\cdot}H_2O$ caused the occurrence of a phase evolution from anatase-rich samples into $Li_4Ti_5O_{12}$-TiO_2 rutile nanocomposites. Also, the XRD findings demonstrated the lattice expansion of LTO owing to increased Li-doping through the addition of higher contents of $LiOH{\cdot}H_2O$.
(2) Quantitative analysis of XRD results indicated that the crystallite size of the LTO phase of the samples first increased to a maximum value of 47.3 nm and then decreased to 20–21 nm by the addition of higher ratios of $LiOH{\cdot}H_2O$: TBT. Consequently, LTO phase content rose sharply from 6.7% to 97.23%, while the TiO_2 anatase decreased from 89.36% to 0.2%, and minor rutile TiO_2 (2.55–4.9%).
(3) The morphological analyses of samples revealed that when the $LiOH{\cdot}H_2O$: TBT ratio was 4:5, the average particle size was 138 nm (related to TiO_2 anatase). By increasing the $LiOH{\cdot}H_2O$ content, a mixture of sheet-like and near-spherical morphologies with an average particle size of 196 nm was achieved. At high $LiOH{\cdot}H_2O$ content, particle growth was inhibited, and particles with an average size of 55 nm were formed. Accordingly, it can be deduced that by increasing the $LiOH{\cdot}H_2O$ content, initially

particle size increased (at low ratios like 4:5, 6:5, promoting TiO_2 anatase growth) while at higher ratios (10:5, 12:5), growth was prevented and a phase evolution to LTO and TiO_2 rutile occurred.

(4) In summary, for defect-engineered LTO-TiO_2 rutile with small particles, the higher ratios of $LiOH{\cdot}H_2O$: TBT are recommended.

While this work provides a comprehensive structural and morphological map of LTO-TiO_2 nanocomposites synthesized under highly Li-excess conditions, we acknowledge that electrochemical characterization is necessary to assess the practical value of these materials as battery anodes. The ultrafine nanoparticles obtained in the LT-10-5 sample (55 nm, 95% LTO) and the high-purity LTO phase in the LT-12-5 represent particularly promising candidate structures for future charge/discharge and rate-capability studies.

CRediT authorship contribution statement

Hamed Aghamohammadi: Writing – review & editing, Writing – original draft, Methodology, Investigation. **Atousa Khazaeli:** Methodology, Investigation. **Reza Eslami-Farsani:** Supervision.

Declaration of competing interest

The authors declare that they have no known competing financial interests or personal relationships that could have appeared to influence the work reported in this paper.

References

Aghamohammadi, H., & Eslami-Farsani, R. (2022). Synthesis and electrochemical performance of TiNb2O7 nanoparticles grown on electrochemically prepared graphene as anode materials for Li-ion batteries. *Journal of Power Sources, 535*, Article 231418.

Aghamohammadi, H., Eslami-Farsani, R., & Oskouei, H. I. (2024). Electrochemical performance of TiNb2O7/graphene/CNTs hybrid nanocomposites as anode materials for Li-ion batteries. *Diamond and Related Materials, 141*, Article 110654.

Aghamohammadi, H., Hassanzadeh, N., & Eslami-Farsani, R. (2021). A review study on titanium niobium oxide-based composite anodes for Li-ion batteries: Synthesis, structure, and performance. *Ceramics International, 47*, 26598–26619.

Ariyoshi, K., Yamato, R., & Ohzuku, T. (2005). Zero-strain insertion mechanism of Li [Li1/3Ti5/3] O4 for advanced lithium-ion (shuttlecock) batteries. *Electrochimica Acta, 51*, 1125–1129.

Challagulla, S., Tarafder, K., Ganesan, R., & Roy, S. (2017). Structure sensitive photocatalytic reduction of nitroarenes over TiO 2. *Scientific Reports, 7*, 8783.

Chen, C., Shi, H., Jiang, H., & Zhu, J. (2025a). Recent progress on titanium niobium oxide as anode material for lithium-ion batteries. *Journal of Electronic Materials*, 1–24.

Chen, C., Shi, H., Jiang, H., & Zhu, J. (2025b). Recent progress on titanium niobium oxide as anode material for lithium-ion batteries. *Journal of Electronic Materials, 54*, 3346–3369.

Gangaja, B., Nair, S., & Santhanagopalan, D. (2024a). *Composite anode for high performance full-cell Li-ion battery and Li-ion capacitor applications*.

Gangaja, B., Nair, S., & Santhanagopalan, D. (2024b). Li4Ti5O12-TiO2 composite anode for high performance full-cell Li-ion battery and Li-ion capacitor applications. *Discover Electrochemistry, 1*, 5.

Ge, H., Li, N., Li, D., Dai, C., & Wang, D. (2008). Study on the effect of Li doping in spinel Li4+ xTi5− xO12 (0⩽ x⩽ 0.2) materials for lithium-ion batteries. *Electrochemistry Communications, 10*, 1031–1034.

Grzmil, B., Kic, B., & Rabe, M. (2004). Inhibition of the anatase-rutile phase transformation with addition of K2O, P2O5, and Li2O. *Chemical Papers, 58*, 410–414.

Hanaor, D. A., Assadi, M. H., Li, S., Yu, A., & Sorrell, C. C. (2012). Ab initio study of phase stability in doped TiO2. *Computational Mechanics, 50*, 185–194.

He, Y. F., Chu, D. Y., & Zhuo, Z. (2021). Cycle stability of dual-phase lithium titanate (LTO)/TiO2 nanowires as lithium battery anode. *Journal of Multidisciplinary Applied Natural Science, 1*, 54–61.

Hu, X., Wu, Y., Zou, Y., & Yang, G. (2024). The formation mechanism of NaLiTi3O7 and its effect on Li4Ti5O12 prepared by the NaCl molten salt flux method. *Ceramics International, 50*, 10285–10291.

Hwang, C. H., Kim, H.-e., Nam, I., & Bang, J. H. (2019). Polygonal multi-polymorphed Li4Ti5O12@ rutile TiO2 as anodes in lithium-ion batteries. *Nano Research, 12*, 897–904.

Kazemi, A., Mostaani, R., Ravari, M. K., Ghorbanzadeh, M., Yavarinasab, M., Enferadi, J., Chen, Z., Iqbal, N., Xiang, Y., & Liu, W. (2025). Enhancing high rate performance of lithium titanium oxide (LTO) anodes: A comprehensive review. *Journal of Power Sources, 630*, Article 236051.

Kim, S. A., Hussain, S. K., Abbas, M. A., & Bang, J. H. (2022). High-temperature solid-state rutile-to-anatase phase transformation in TiO2. *Journal of Solid State Chemistry, 315*, Article 123510.

Kuo, Y.-C., & Lin, J.-Y. (2014). One-pot sol-gel synthesis of Li4Ti5O12/C anode materials for high-performance Li-ion batteries. *Electrochimica Acta, 142*, 43–50.

Li, B., Han, C., He, Y.-B., Yang, C., Du, H., Yang, Q.-H., & Kang, F. (2012). Facile synthesis of Li 4 Ti 5 O 12/C composite with super rate performance. *Energy & Environmental Science, 5*, 9595–9602.

Li, N., Mei, T., Zhu, Y., Wang, L., Liang, J., Zhang, X., Qian, Y., & Tang, K. (2012). Hydrothermal synthesis of layered Li 1.81 H 0.19 Ti 2 O 5· x H 2 O nanosheets and their transformation to single-crystalline Li 4 Ti 5 O 12 nanosheets as the anode materials for Li-ion batteries. *CrystEngComm, 14*, 6435–6440.

Liu, K., Cui, J., Yin, J., Man, J., Cui, Y., Wen, Z., & Sun, J. (2018). Ultra-long life core-shell structure Li4Ti5O12/C nanocomposite anode materials for lithium ion batteries. *Journal of Alloys and Compounds, 765*, 229–235.

Merazga, S., Boudeffar, F., Rahal, B., Berouaken, M., Mebarki, M., Ayouz, K., Ayat, M., & Gabouze, N. (2024). Thermal annealing effect on hydrothermal synthesized Li4Ti5O12/TiO2 as anode material for lithium-ion batteries. *Journal of the Electrochemical Society, 171*, Article 040541.

Michalska, M., Pavlovsky, J., Peikertova, P., Holesova, S., Anuratha, K. S., & Lin, J.-Y. (2022). Mesoporous/Microporous Li4Ti5O12/rutile-TiO2 as an anode material for lithium-ion batteries synthesized by the sol-gel method. *Solid State Ionics, 384*, Article 116005.

Muzayanha, S. U., Purwanto, A., Putra, M. I., & Aliwarga, H. K. (2021). The effect of modified LTO synthesis using salt assisted method with various of salt metal materials. In *, 1117. IOP conference series: Materials science and engineering*. IOP Publishing, Article 012022.

Parikh, D., Geng, L., Lyu, H., Jafta, C. J., Liu, H., Meyer III, H. M., Chen, J., Sun, X.-G., Dai, S., & Li, J. (2021). Operando analysis of gas evolution in TiNb2O7 (TNO)-based anodes for advanced high-energy lithium-ion batteries under fast charging. *ACS Applied Materials & Interfaces, 13*, 55145–55155.

Rahman, M. M., Wang, J.-Z., Hassan, M. F., Liu, H. K., & Wexler, D. (2011). Amorphous carbon coated high grain boundary density dual phase Li {sub 4} Ti {sub 5} O {sub 12}-TiO {sub 2}: a nanocomposite anode material for Li-ion batteries. *Advanced Energy Materials, 1*.

Shen, C.-m., Zhang, X.-g., Zhou, Y.-k., & Li, H.-l. (2003). Preparation and characterization of nanocrystalline Li4Ti5O12 by sol–gel method. *Materials Chemistry and Physics, 78*, 437–441.

Sushko, M. L., Rosso, K. M., & Liu, J. (2010). Mechanism of Li+/electron conductivity in rutile and anatase TiO2 nanoparticles. *Journal of Physical Chemistry C, 114*, 20277–20283.

Tran, M., Huynh, N., Nguyen, T., Ha, D., & Le, P. (2016). Facile solution route to synthesize nanostructure Li4Ti5O12 for high rate Li-Ion battery. *Journal of Nanomaterials, 2016*, Article 4261069.

Winowatan, P. W., Selwyn, S., Priyono, B., & Syahrial, A. Z. (2021). Enhancing battery performance of Li4Ti5O12 nanorod synthesized by hydrothermal method with Sn addition as anode material for lithium-ion battery. *Journal of King Saud University, Engineering Sciences, 33*, 396–403.

Wu, L., Leng, X., Liu, Y., Wei, S., Li, C., Wang, G., Lian, J., Jiang, Q., Nie, A., & Zhang, T.-Y. (2017). A strategy for synthesis of nanosheets consisting of alternating spinel Li4Ti5O12 and rutile TiO2 lamellas for high-rate anodes of lithium-ion batteries. *ACS Applied Materials & Interfaces, 9*, 4649–4657.

Wu, Y., Zeng, Y., Wang, R., Zou, Y., Zhang, Y., Zhang, S., & Yang, G. (2025). One-step solid-state synthesis of truncated octahedral Mo-doped Li4Ti5O12 for Li-ion batteries. *Journal of Alloys and Compounds*, Article 180941.

Xie, Z., Song, Q., Xie, H., Yin, H., & Ning, Z. (2021). Chemically driven synthesis of Ti3+ self-doped Li4Ti5O12 spinel in molten salt. *Journal of the American Ceramic Society, 104*, 753–765.

Xu, H., Chen, J., Li, Y., Guo, X., Shen, Y., Wang, D., Zhang, Y., & Wang, Z. (2017). Fabrication of Li4Ti5O12-TiO2 nanosheets with structural defects as high-rate and long-life anodes for lithium-ion batteries. *Scientific Reports, 7*, 2960.

Xue, B., Wang, K., Tan, Y., Li, Q., & Sun, J. (2019). Fabrication and performance of Li4Ti5O12/cotton-driven carbon fiber as anode for lithium-ion batteries. *Ionics, 25*, 2535–2542.

Zhang, H., Yang, Y., Xu, H., Wang, L., Lu, X., & He, X. (2022). Li4Ti5O12 spinel anode: Fundamentals and advances in rechargeable batteries. *InfoMat, 4*, Article e12228.

Zhang, E., & Zhang, H. (2019). Hydrothermal synthesis of Li4Ti5O12-TiO2 composites and Li4Ti5O12 and their applications in lithium-ion batteries. *Ceramics International, 45*, 7419–7426.

Zhang, Y., Zhang, Y., Huang, L., Zhou, Z., Wang, J., Liu, H., & Wu, H. (2016). Hierarchical carambola-like Li4Ti5O12-TiO2 composites as advanced anode materials for lithium-ion batteries. *Electrochimica Acta, 195*, 124–133.

Zhu, J., Zhang, Y., Zhu, J., Duan, R., & Da, Y. (2016). Hydrothermal synthesis of Li4-xNaxTi5O12 and Li4-xNaxTi5O12/graphene composites as anode materials for lithium-ion batteries. In *MATEC web of conferences, 65*. EDP Sciences, Article 02008.

Zima, T., Ukhina, A., & Uvarov, N. (2023). Formation of nanostructured Li4Ti5O12-Based composites upon hydrothermal treatment of their components. *Inorganic Materials, 59*, 957–963.

Zou, Y., Li, L., Zhang, Y., & Yang, G. (2025). Effects of TiO2 on the performance of Li4Ti5O12 prepared by solid-state method. *Solid State Ionics, 431*, Article 117036.